

Role of Divalent Metal Cations in ATP Hydrolysis Catalyzed by the Hepatitis C Virus NS3 Helicase: Magnesium Provides a Bridge for ATP to Fuel Unwinding

David N. Frick*, Sukalyani Banik and Ryan S. Rypma

Department of Biochemistry and Molecular Biology, New York Medical College, Valhalla, NY 10595, USA

This study investigates the role of magnesium ions in coupling ATP hydrolysis to the nucleic acid unwinding catalyzed by the NS3 protein encoded by the hepatitis C virus (HCV). Analyses of steady-state ATP hydrolysis rates at various RNA and magnesium concentrations were used to determine values for the 15 dissociation constants describing the formation of a productive enzyme–metal–ATP–RNA complex and the four rate constants describing hydrolysis of ATP by the possible enzyme–ATP complexes. These values coupled with direct binding studies, specificity studies and analyses of site-directed mutants reveal only one ATP binding site on HCV helicase centered on the catalytic base Glu291. An adjacent residue, Asp290, binds a magnesium ion that forms a bridge to ATP, reorienting the nucleotide in the active site. RNA stimulates hydrolysis while decreasing the affinity of the enzyme for ATP, magnesium, and MgATP. The binding scheme described here explains the unusual regulation of the enzyme by ATP that has been reported previously. Binding of either free magnesium or free ATP to HCV helicase competes with MgATP, the true fuel for helicase movements, and leads to slower hydrolysis and nucleic acid unwinding.

© 2006 Elsevier Ltd. All rights reserved.

*Corresponding author

Keywords: ATPase; metal ions; viral RNA replication; enzyme mechanism

Introduction

Helicases are motor proteins that travel along nucleic acid tracks to separate a double helix, rearrange secondary structures, assist homologous strand exchange, or strip proteins from DNA or RNA. All known helicases are fueled by the hydrolysis of nucleoside triphosphates (NTPs) in a process that is assisted by divalent metal cations. ATP binds helicases at a Walker-type (P-loop) nucleotide-binding site that is formed by two conserved sequence motifs.¹ The helicase examined here is encoded by the hepatitis C virus (HCV). HCV is a positive-sense RNA virus that encodes a large

polyprotein that is processed into both structural and non-structural proteins. The non-structural HCV proteins form a viral replicase that synthesizes new viral RNA directly from RNA templates. The HCV helicase is required for HCV replication most likely by virtue of its ability to track along RNA and resolve double-stranded intermediates as it does *in vitro*,² as evidenced by the fact that HCV helicase stimulates the HCV RNA polymerase,³ and because subgenomic replicons without a functional helicase synthesize and process viral polyproteins but fail to synthesize additional RNA.⁴ There are many other possible roles for HCV helicase, however, such as in assisting translation, protein processing, packaging RNA into virions, and in transporting the NS3–NS4A protease to cellular targets. Nevertheless, because HCV cannot replicate its RNA without a functional NS3 helicase,⁴ the enzyme is considered a possible target for new drugs needed to treat a disease affecting 2% of the world's population.^{5–7} The goal of this study is to understand precisely how metal ions help ATP fuel HCV helicase action.

Abbreviations used: HCV, hepatitis C virus; NS3, non-structural protein 3; NS4A, non-structural protein 4A; FRET, fluorescence resonance energy transfer.

E-mail address of the corresponding author:
David.Frick@NYMC.edu

In HCV infected cells, non-structural proteins 3 (NS3) and 4A (NS4A) form the viral helicase. The NS3–NS4A complex cleaves the viral polyprotein at four sites,^{8,10} hydrolyzes ATP,⁹ and uses the energy derived from ATP hydrolysis to unwind RNA.¹¹ Unlike related RNA helicases, HCV helicase is also a potent DNA helicase.¹² The protease portion of NS3 that binds NS4A and cleaves the polyprotein comprises amino acid residues 1–166, and the minimum helicase comprises 167–631. A truncated NS3 fragment lacking the protease region retains most of its DNA helicase activity but unwinds RNA poorly compared with the full-length NS3–NS4A complex.¹³

To date, the crystal structure of HCV helicase has been determined by five separate groups. Two structures show monomeric NS3 helicase fragments isolated from HCV genotypes 1a¹⁷ and 1b.¹⁴ One shows a monomer of genotype 1a helicase bound to a DNA oligonucleotide,¹⁵ and another shows the full length NS3 protein.¹⁶ The C-terminal helicase portion of NS3 is made of three domains.^{14–17} The two N-terminal domains contain conserved motifs and resemble the core domain of the recombination protein RecA.¹⁸ The first and second helicase motifs in the N-terminal RecA like domain are the Walker A and B motifs. One strand of nucleic acid binds in the cleft separating RecA-like domains 1 and 2 from a third domain which does not resemble any domains seen in other helicase structures.¹⁵

The most recent HCV helicase structure, in contrast, shows two NS3 helicase fragments bound to a single oligonucleotide,¹⁹ and there is presently much debate over whether the individual subunits in a NS3 oligomer coordinate their actions to unwind RNA. Early transient state kinetic analyses of HCV helicase supported the notion that HCV helicase moves with a step size of 1–2 bp and that the protein functions as a monomer.²⁰ However, when Levin *et al.* repeated the same basic experiment, they found a much larger (9 bp) step size and they observed “the functional interaction of the hepatitis C virus helicase molecules,” which is more indicative of a dimeric protein.²¹ Tackett *et al.* repeated the kinetic analysis of HCV helicase-catalyzed DNA unwinding for a third time using the full-length NS3 protein rather than the truncated NS3 helicase fragment and noted even more subunit cooperativity.²² About the same time, Serebrov & Pyle developed a novel RNA-based assay, which allowed the progress of a helicase along a long RNA strand to be monitored. The RNA-based assay again showed that the functional unit of NS3 is a dimer, and that it unwinds with a large step size (18 bp). That study also showed that NS3 pauses while moving along the RNA.²³ This periodic cycle of pausing and unwinding was recently confirmed in a collaborative study using optical tweezers to examine the action of single molecules of NS3 on RNA.² Notably, this single molecule study did not confirm that NS3 oligomerizes to unwind RNA.

Even though RNA/DNA unwinding by HCV helicase has been well characterized, how ATP binding and hydrolysis propels the helicase is still not known. Indeed, there is some confusion in the HCV literature regarding exactly how many ATP binding sites there are on each NS3 protein,²⁴ whether or not adjacent subunits in nucleic acid-bound NS3 oligomers bind ATP cooperatively,²⁵ and even the absolute requirement of ATP for unwinding.²⁶ In the atomic structures of other helicases,^{27–30} non-hydrolyzable NTP analogs are always seen bound between two RecA-like domains¹⁸ with a divalent metal cation linking the β and γ phosphates with the Walker B motif on one RecA-like domain. Because such structures differ from those seen in the absence of NTPs in that the RecA-like domains are rotated differently, it is widely assumed that NTP-induced domain rotation leads to helicase movement. The available HCV NS3 structures reveal that the second RecA-like domain could rotate upon ATP or RNA binding,^{14–17,19} but an atomic structure of HCV helicase has not yet been visualized with bound NTPs. It is therefore important to examine how and where Mg^{2+} and ATP bind HCV helicase, and how these interactions influence the relationship between the helicase and the RNA on which it is moving.

Based on the structures of similar proteins,^{29,30} we propose that Mg^{2+} coordinates the β and γ phosphates of ATP with an aspartate near the catalytic base, activating a nucleophilic water molecule. We show here using site-directed mutagenesis, that NS3 residues D290 and E291 in conserved motif II (the Walker B motif) serve as the metal binding residue and catalytic base, respectively. We also show that HCV helicase binds and hydrolyzes ATP in the absence of divalent metal cations. In the absence of metal, hydrolysis occurs at the Walker site with E291 functioning as a catalytic base, and ATP binds more weakly than it does in the presence of metal. In the absence of metal, HCV helicase binds some NTPs more tightly than others and as a result some NTPs are hydrolyzed more slowly than ATP, particularly those with hydrogen atoms at position N1 of the purine. Global non-linear least-squares analysis of steady-state rates of ATP hydrolysis in the absence or presence of various concentrations of Mg^{2+} and ATP was used to determine all 15 equilibrium constants describing the binding of ATP and two activators (Mg^{2+} and RNA) to the HCV helicase. The data support a model in which Mg^{2+} forms a bridge between D290 and ATP and reorients the NTP in the active site so that it is more rapidly hydrolyzed. When RNA binds, ATP hydrolysis is further accelerated, but Mg^{2+} (and likewise ATP or $MgATP$) binds more weakly to the enzyme. Thus, a RNA-induced conformational change is directly linked to $MgATP$ binding and ATP hydrolysis. Finally, we show that since only the enzyme– Mg^{2+} –ATP complex is capable of moving along RNA, binding of either free NTPs or free Mg^{2+} inhibit the biological function of HCV helicase.

Results

The purpose of this study was to examine the role of divalent metal ions in the HCV helicase-catalyzed reaction. As others previously noted,^{12,31–33} we observed that HCV helicase catalyzed RNA (and DNA) unwinding absolutely requires divalent metal cations. However, we were surprised to find that in the absence (or presence) of RNA (or DNA), HCV helicase–protease complex did not require Mg^{2+} to hydrolyze ATP (Figure 1(a)). We made this discovery after finding that the addition of EDTA (up to 10 mM) did not terminate ATP hydrolysis. Because the full-length NS3–NS4 complex frequently co-purifies with a zinc ion bound to the protease domain of NS3,¹⁶ it is possible that metal ions that co-purify with the protease portion of NS3 were stimulating hydrolysis. We therefore repeated the measurements with truncated NS3 proteins lacking the NS3 protease, each of which was purified in the presence of EDTA. Each truncated NS3 protein was isolated from a different viral genotype (1a-H77, 1b-J4, and 2a-J6), and because of this genetic variability, they each hydrolyzed ATP at somewhat different rates in the absence of RNA.³⁴ However, each protein retained an ability to hydrolyze ATP without metal at rates about one-third of those seen in the presence of Mg^{2+} (Figure 1(b)).

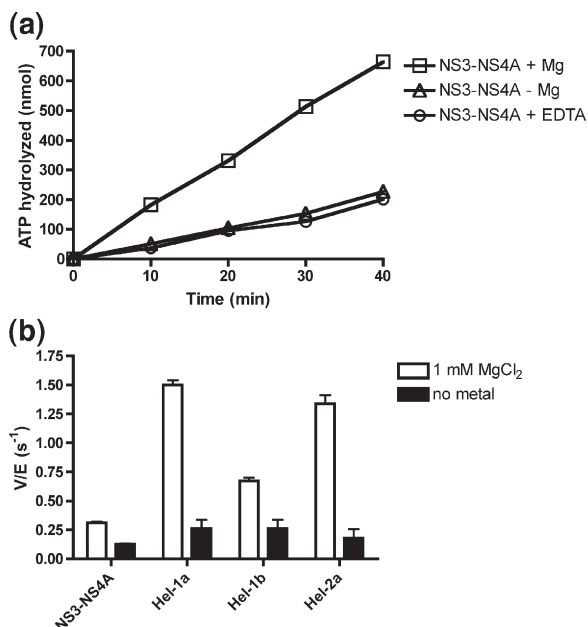


Figure 1. HCV helicase-catalyzed ATP hydrolysis in presence and absence of magnesium. (a) Time course for ATP hydrolysis catalyzed by the HCV NS3–NS4A complex in the presence of 5 mM $MgCl_2$ (squares), in the absence of $MgCl_2$ (triangles) and in the presence of 1 mM EDTA. (b) Specific activity (nmol ATP hydrolyzed/s per nmol protein) of the NS3–NS4A protein complex and the truncated NS3 protein lacking the protease regions purified in the presence of EDTA from three different HCV genotypes.³⁴ Error bars represent standard deviations from 12 separate velocity measurements.

Specificity of the metal independent HCV helicase NTPase

In the presence of Mg^{2+} , HCV helicase cleaves all eight canonical (d)NTPs with similar turnover rates although ATP has a somewhat lower K_m value than CTP and UTP, which are in turn better substrates than GTP.³⁴ Since the K_m values of all NTPs are quite low in the presence of Mg^{2+} (1–20 μM), each was cleaved at relatively the same rate when they were present at 1 mM in the reaction mixture (Figure 2(a)). This relative non-specific cleavage changed dramatically, however, when divalent metal cations were not present in the reaction (Figure 2(b)).

In the absence of metals, ATP and CTP were cleaved faster than UTP or GTP (Figure 2(b)). GTP was not hydrolyzed at a detectable rate. Importantly, this specificity did not change when EDTA was added to absorb metal that might be contaminating the NTP solutions. Identical rates for each of the NTPs were obtained either in the absence of EDTA or when EDTA was added up to a concentration of 2 mM (data not shown). The data reveal that in the presence of metal, the enzyme does not discriminate on the basis of the nucleotide base. However, in the absence of metal, the enzyme more closely examines the base. It is important to note that in the presence of metal the rates in Figure 2(a) approximately reflect the V_{max} values because the enzyme is almost saturated with NTP and metal, while in the absence of metal, the rates are not near the V_{max} because NTPs bind weaker without metal (see data below).

We used purine analogs to examine the specificity of the metal-independent HCV NS3 NTPase in more detail. As shown in Figure 2(c), those NTPs that possess a carbonyl group at the 6 position of the purine were hydrolyzed at a lower rate. The 2-amino group of guanine appeared also deleterious, because xanthosine triphosphate was hydrolyzed faster than GTP. Blocking the ability of the 2-oxo group to act as a hydrogen bond acceptor led to faster hydrolysis. However, blocking the 6-amino group with a methyl did not affect hydrolysis. One common feature of all the NTPs that were hydrolyzed relatively well is that the purine N1 position (or pyrimidine N3) is not protonated, meaning it can act as hydrogen bond acceptor. In contrast in poor substrates, purine N1 is typically protonated, acting as hydrogen bond donor (arrows in Figure 2(c)). Thus, it appears that in the absence of metals HCV helicase forms specific contacts with the moieties that form Watson–Crick hydrogen bonds. However, in the presence of metal, contacts between the enzyme and the nucleotide base do not affect NTP binding or hydrolysis. Although it was not possible to perform a complete analysis with all analogs because of their availability and purity, the differences in specificity in the absence of metal are likely due to both V_{max} and K_m effects, since at 1 mM, the protein is not saturated with NTPs and because

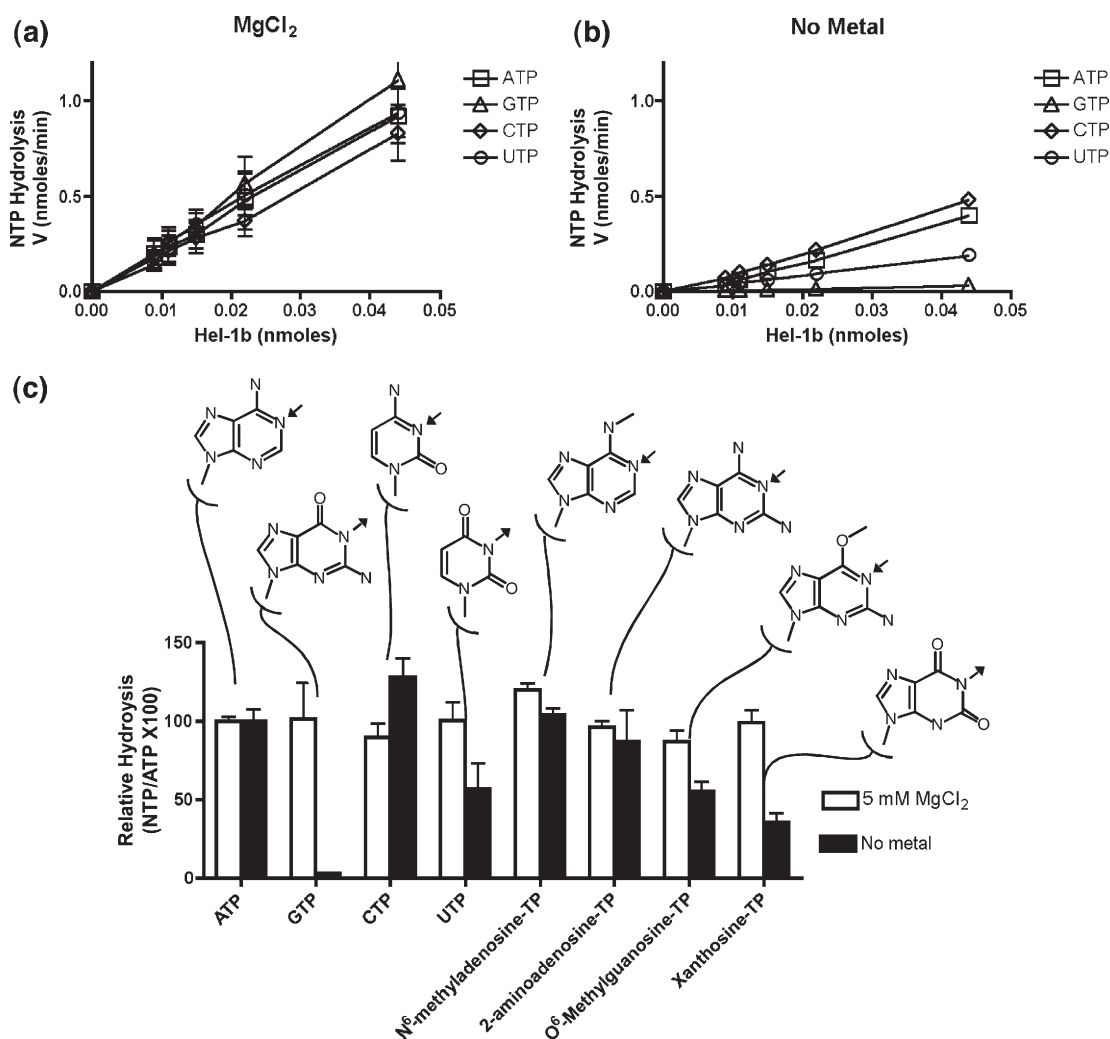


Figure 2. Hydrolysis of various nucleoside triphosphates by HCV helicase in the presence and absence of Mg²⁺. (a) HCV helicase catalyzed hydrolysis of ATP (squares), GTP (triangles), CTP (diamonds), and UTP (circles) in the presence of 5 mM MgCl₂. (b) HCV helicase catalyzed hydrolysis of ATP (squares), GTP (triangles), CTP (diamonds), and UTP (circles) in the absence of divalent metal cations. (c) Relative hydrolysis rates in the presence (white bars) and absence (black bars) of MgCl₂. Each NTP was present at an initial concentration of 1 mM. Error bars represent standard deviations from eight separate velocity measurements. Note that those NTPs where purine N1 (or pyrimidine N3) acts as a hydrogen bond acceptor are hydrolyzed faster than those with a hydrogen atom in that position (see arrows).

some NTPs bind notably weaker in the absence of metal (see data below for ATP and GTP).

Metal-independent hydrolysis occurs at the Walker ATP-binding site

In all enzymes that utilize a Walker-type nucleotide-binding site to hydrolyze NTPs, the true substrate is usually MgATP or a similar metal-NTP complex. It was therefore quite surprising that HCV helicase could hydrolyze NTPs in the absence of metal. Reports of metal-independent NTP binding to helicase have been rare. The T7 helicase binds NTPs in the absence of metal,³⁵ but this ring helicase is evolutionarily only distantly related to HCV helicase. A closely related helicase from Dengue virus was reported to remove the terminal phosphate from a triphosphate linked to RNA without

added metal,^{36,37} but a subsequent analysis revealed that metal is needed for Dengue helicase catalyzed hydrolysis.³⁸ NTP binding and hydrolysis at the Walker-NTP binding site of HCV helicase in the absence of metal would therefore be a very unusual property.

One possible explanation for metal-independent ATP hydrolysis by HCV helicase is that free ATP could bind to HCV helicase at a second site, distinct from the Walker site and which hydrolyzes ATP at a slow rate. Others have proposed a second allosteric ATP binding site on HCV helicase,^{24,25} and the fact that the NTP specificity changes without metal indirectly supports this contention. A second, explanation for the metal-independent ATP hydrolysis reported here is that the enzyme preparations were contaminated with another enzyme that does not require metal to hydrolyze NTPs. In order to determine if the metal independent hydrolysis

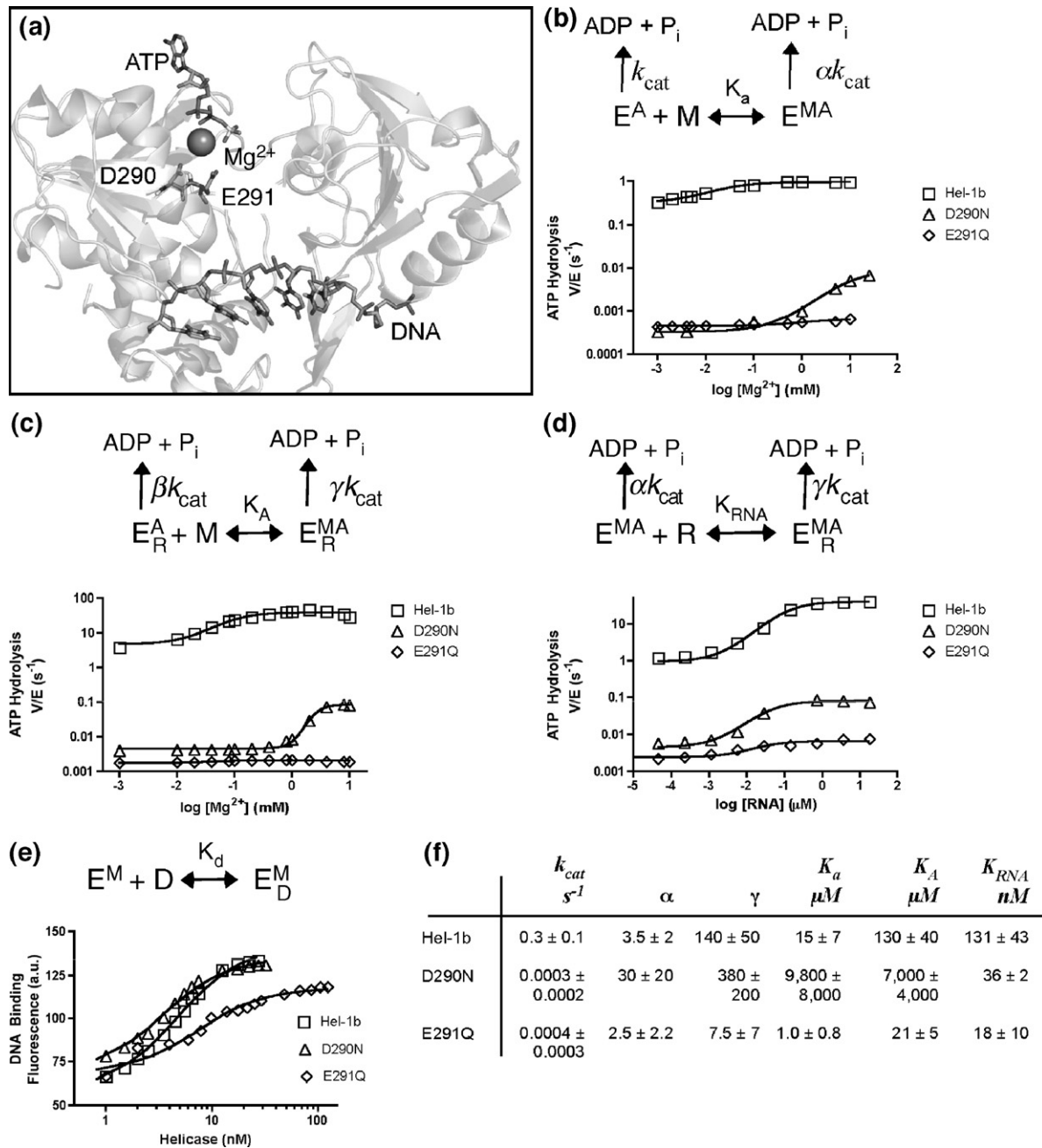


Figure 3. Roles of NS3 residues D290 and E291 in ATP hydrolysis. (a) Alignment of the HCV helicase-oligonucleotide structure (PDB file 1A1V)¹⁵ with the structure of the RecQ helicase bound to ATP- γ S (PDB file 1OYY).²⁹ Shown are the DNA and protein from 1A1V, with D290 and E291 as sticks, and the Mn^{2+} and ATP- γ S from 1OYY. (b) $MgCl_2$ activation of ATP hydrolysis (2 mM initial ATP concentration) catalyzed by wild-type Hel-1b (squares), D290N (triangles) and E291Q (diamonds). (c) $MgCl_2$ activation of ATP hydrolysis in the presence of 1 mM poly(U) RNA catalyzed by wild-type Hel-1b (squares), D290N (triangles) and E291Q (diamonds). (d) RNA activation of ATP hydrolysis in the presence of 5 mM $MgCl_2$. (e) Titrations of a fluorescein labeled oligonucleotide (2 nM) with Hel-1b (squares), D290N (triangles) and E291Q (diamonds). (f) Data in (b) to (e) were fit to one-site binding equations to yield the rate and equilibrium constants defined in each panel. Uncertainties include the range of values obtained after three repeat titrations.

results from a second site or a contaminating enzyme, two directed mutants of HCV helicase were generated and purified using the exact same procedure as was used for the wild-type enzyme (Figure 3(a)).

The first mutant analyzed contained substitutions that coded for the replacement of D290, an aspartate

in the Walker B sequence that putatively binds the metal. Accordingly, loss of D290 should lead to a protein that binds Mg^{2+} more weakly. The mutant protein, called D290N, contained an asparagine in place of the aspartate. An Asn is similar in size to an Asp but cannot coordinate cations because it is not ionizable. The second mutant protein contained a

glutamine in place of E291. The homologous residue in other helicases has been shown to be a catalytic base.³⁹ In this mutant, Glu was replaced with Gln. Gln cannot accept protons, so if this amino acid functions as a catalytic base, the E291Q mutant should be a profoundly worse catalyst compared to the wild-type enzyme.

We found that neither D290N nor E291Q unwind DNA or RNA in any standard assays (as reported by others),⁴⁰ but each protein retained some ability to cleave ATP. Analysis of ATP hydrolysis catalyzed by D290N and E291Q clearly demonstrates that the Walker-site on the HCV helicase is responsible for both metal-dependent and metal-independent ATP hydrolysis (and that a contaminating protein is not hydrolyzing ATP). First, both mutants are profoundly deficient in catalyzing ATP hydrolysis both in the presence and absence of Mg^{2+} (Figure 3(b) and (f)). In the absence of Mg^{2+} both cleave ATP about 1000 times slower than wild-type (Figure 3(b), (c) and (f)). Mg^{2+} stimulates ATP hydrolysis by both mutants, but the D290N mutant binds Mg^{2+} about 650 times weaker than wild-type (compare K_a values; Figure 3(b) and (f)). In contrast, less Mg^{2+} was needed to stimulate E291Q than wild-type, implying that E291 does not normally coordinate metal ions (Figure 3(b), (c) and (f)). RNA stimulates hydrolysis of both mutants (Figure 3(d)), and in the presence of RNA, D290N binds Mg^{2+} 71 times more weakly than wildtype (compare K_A values; Figure 3(c) and (f)). Both D290N and E291Q bind RNA as tightly as wild-type, as revealed by the fact that the amount of RNA needed to stimulate 50% maximal

rates of ATP hydrolysis (K_{RNA}) for each mutant is similar to that need to stimulate the wild-type (Figure 3(d) and (f)).

One possible explanation for the profound defects seen in E291Q and D290N, neither of which unwinds DNA or RNA under any conditions tested (data not shown) is that the mutant proteins are not folded properly. If this were the case then an active site titration would reveal that vastly more ligands would be necessary to saturate the enzyme. We therefore titrated each protein into a solution of 2 nM of a DNA oligonucleotide (about 6–9 nM binding sites assuming three protein molecules bind each oligonucleotide). Because the wild-type helicase binds this oligonucleotide stoichiometrically with a sub-nanomolar K_d , the inflection point of the titration curve roughly reveals the amount of binding sites.¹³ The titrations revealed that D291Q binds DNA with the same stoichiometry as wild-type and the E2901Q preparation contains no less than half the binding sites as the wild-type. Both mutants bound the DNA tightly with a K_d values in the sub-nanomolar range (Figure 3(e)).

Equilibrium model for Mg^{2+} , ATP, and RNA binding to HCV helicase

Since ATP appears to bind to the same site both in the presence and absence of Mg^{2+} , a model can be used to relate the dissociation constants explaining the formation of an enzyme–metal–ATP–RNA complex. As described by Segel,⁴¹ an equilibrium

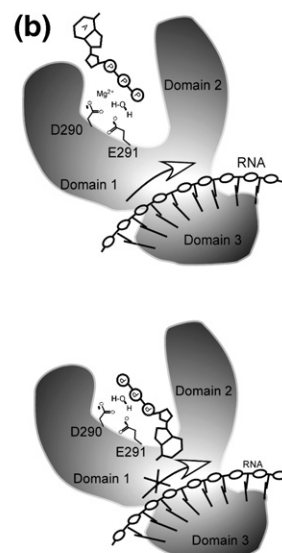
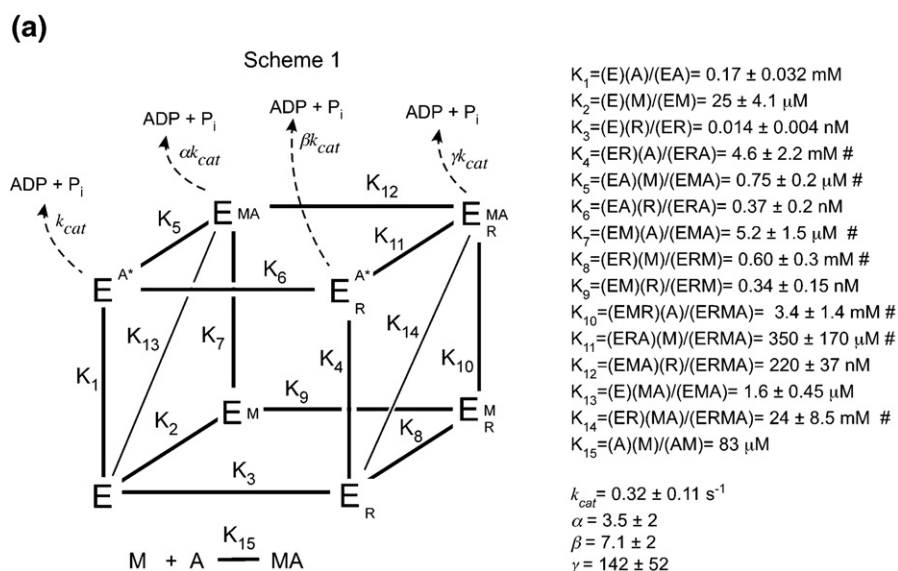


Figure 4. Scheme for binding of ATP, Mg^{2+} , and RNA to HCV helicase. (a) Binding of the substrate (ATP) and two activators (Mg^{2+} , RNA) can be described by a minimum of 15 dissociation constants assuming that Mg^{2+} binds ATP in the absence of enzyme and that Mg^{2+} binding to RNA does not influence the affinity of RNA for the enzyme. Definitions of each constant are shown with values resulting from global non-linear regression analysis of steady-state rates and DNA binding assays (see Materials and Methods). K_{15} was from Williams *et al.*⁵³ Constants calculated from others are noted (#) (b) Diagrams of ATP coordination in the presence (top) and absence of divalent metal cations. In the presence of metal, ATPs are likely bonds as shown in Figure 3(a) with the enzyme making few contacts with the base. In the absence of metal, the enzyme more selectively binds and hydrolyzes NTPs, by making contacts with the edge of the base needed for Watson–Crick base-pair formation.

binding model for an enzyme with two activators resembles a cube with its sides made of 12 dissociation constants describing the formation of the binary complexes (enzyme–ATP, enzyme–Mg²⁺, and enzyme–RNA), ternary complexes (enzyme–Mg²⁺–ATP, enzyme–Mg²⁺–RNA, and enzyme–ATP–RNA), and the quaternary complex enzyme–Mg²⁺–ATP–RNA (Scheme 1; Figure 4(a)). In addition, since metal can bind ATP in the absence of enzyme, three additional constants are needed to describe this event and the binding of MgATP to free enzyme or an enzyme RNA complex. The diagonals on the side of the cube dictate binding of a pre-formed MgATP complex to either enzyme alone (K_{13}) or an enzyme–RNA complex (K_{14}). MgATP forms spontaneously with a dissociation constant (K_{15}) of 83 μM at pH 6.5.⁵³ When the helicase is titrated with ATP and RNA in the presence of Mg²⁺, the enzyme can cycle between six states as defined by the backside and the diagonal plane of Scheme 1 (Figure 4(a)). Each of the four possible enzyme–ATP complexes hydrolyses ATP at a different rate. The basal rate of ATP hydrolysis can be described by a first-order rate constant (k_{cat}). Under saturating conditions, Mg²⁺ activates k_{cat} by a factor α , RNA stimulates by a factor called β , and together RNA and ATP stimulate by a γ factor. Since ATP appears to bind in a different orientation in the absence of metal based on substrate specificity (Figure 3), the enzyme ATP complexes without metal in scheme 1 are noted with an asterisk (i.e. E^{A*}). Sketches of the MgATP and RNA binding sites on HCV helicase and the E^{A*} complex are presented in Figure 4(b). We have chosen to depict the E^{A*} complex with the NTP rotated by 180° solely for dramatic effect. While this conformation is possible based on modeling studies (data not shown), it is equally likely that a more subtle difference between the E^{MA} and E^{A*} structure accounts for the differences in NTP specificity.

The easiest place to start addressing this cubic system (Scheme 1; Figure 4(a)) is on its front side, which describes the binding of ATP and RNA to two independent sites, in the absence of metal. The constant K_1 describes the binding of ATP in the absence of metal, and can be estimated by measuring the K_m of ATP under in the absence of Mg²⁺ or RNA. Repeated ATP titrations in the absence of metal fit to the Michaelis–Menten equation revealed a K_m of 170(\pm 32) μM and a k_{cat} of 0.32(\pm 0.1) s⁻¹. The binding of nucleic acid to the enzyme in the absence of metal can be estimated by titrating a solution containing a fluorescently labeled DNA oligonucleotide with enzyme (Figure 5(a)). Such titrations revealed that each 18-mer binds about three enzyme molecules with a very tight dissociation constant (K_3 in Scheme 1) less than 0.1 nM.

To understand how RNA affects ATP binding and *vice versa*, the enzyme was titrated with both ATP and RNA, and ATP hydrolysis was measured under steady-state conditions. The resulting initial rates were fit to equation (2) (based on Segel's

equation V-1).⁴¹ The data are plotted as a function of RNA concentration along with the best-fit curves resulting from global non-linear regression analysis (Figure 5(b)). The results reveal that ATP binding results in weaker binding of RNA ($K_6 > K_3$). When K_4 was calculated from the relationship $K_1 K_6 / K_3 = K_4$, a weakening of ATP binding in the presence of RNA was revealed ($K_4 > K_1$).

Examination of the dissociation constants defining the backside of the cube reveals both a weaker binding of RNA, and a tighter binding of ATP in the presence of metal. A direct titration of DNA with helicase reveals a K_d of 0.34(\pm 0.15) nM (Figure 5(c)), which corresponds to K_9 in Scheme 1 and is a value significantly weaker than that seen in the absence of Mg²⁺ (Figure 5(a)). When the enzyme was titrated with both ATP and RNA, in the presence of 5 mM MgCl₂, the data could again be fit to a steady-state activation equation (equation (3)). A fit of initial rates obtained in the presence of Mg²⁺ as a function of RNA and ATP concentration are shown along with the best-fit curves in Figure 5(d). A fit to equation (3) reveals clear estimates of αk_{cat} (0.9(\pm 0.4) s⁻¹) and γk_{cat} (45(\pm 20) s⁻¹). In contrast to the global fit performed in the absence of metal, only one constant from Scheme 1 can be determined, because equation (3) describes a simplified binding scheme that does not differentiate between the bindings of ATP (the back edges of the cube) or MgATP (the diagonals on the sides of the cube). Thus to simplify the system, the data were fit using K_{12} and two constants not present in Scheme 1. K_{ATP} (a composite of K_{13} and K_7) represents ATP binding, as ATP or MgATP, in the absence of RNA, and K_{RNA} (a composite of K_3 and K_9) dictates the binding of RNA either to free enzyme or enzyme–metal complex. In the fit, both values were near the respective dissociation constants that were determined as described below (K_{ATP} was 2 μM and K_{RNA} was 3 nM).

Accurately addressing the rest of Scheme 1 was likewise complicated, again, because MgATP forms spontaneously and binds the enzyme in competition with Mg²⁺ and free ATP. As a result, steady-state equations defining the sides of the cube in Scheme 1 (Figure 4(a)) are further complicated because ATP is hydrolyzed in the absence of metal. To simplify the situation, GTP was used as a substrate, because unlike ATP, GTP is not hydrolyzed rapidly by HCV helicase in the absence of metal (Figure 2). GTP is a competitive inhibitor of ATP in the absence of metal with a K_i of 410 μM (Figure 5(e)). If GTP is used as a substrate, k_{cat} can be eliminated from the scheme, and therefore steady-state rates of GTP hydrolysis at different Mg²⁺ concentrations could be fit to equation (4)⁴¹ using the K_i of GTP as K_1 . A fit of the data to equation (4) (Figure 5(f)) revealed both K_{13} (1.6(\pm 0.45) μM) and K_2 (25(\pm 4.1) μM). Since K_2 does not involve the interaction of the enzyme and an NTP, we assumed that this value is the same for ATP as it is for GTP. Similarly, since the helicase displayed little specificity regarding the NTP in the presence of metal, we assumed that K_{13} is likewise

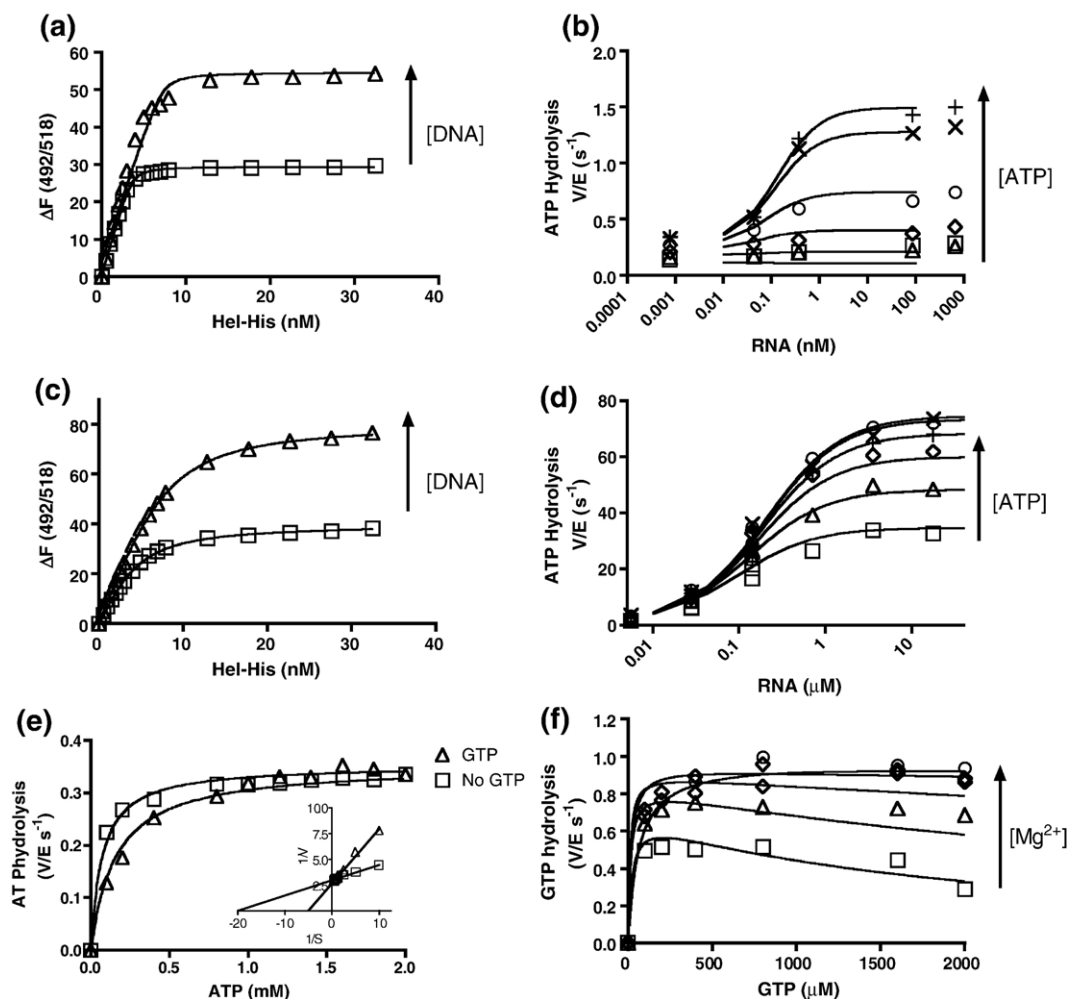


Figure 5. Analysis of the dissociation constants needed to form a HCV helicase–Mg²⁺–ATP–RNA complex and the subsequent turnover rates of ATP hydrolysis. (a) DNA binding in the absence of metal ions. 1 nM (squares) or 2 nM (triangles) of a fluorescein-tagged DNA oligonucleotide were titrated with Hel-1b and change in fluorescence was monitored. Data are fit to equation (1) with a K_d of 0.025 nM and an n of 3.6 protein molecules/oligonucleotide. (b) RNA-stimulated ATP hydrolysis in the absence of metal. Steady-state rates of ATP hydrolysis with initial ATP concentrations of 0.1 mM (squares), 0.2 mM (triangles), 0.4 mM (diamonds), 0.8 mM (circles), 1.6 mM (X), and 2.0 mM ATP (+) at various poly(U) RNA concentrations. Data are fit to equation (2) with the constants listed in Scheme 1 (a). (c) DNA binding in the presence of 5 mM MgCl₂. 1 nM (squares) or 2 nM (triangles) of a fluorescein-tagged DNA oligonucleotide was titrated with Hel-1b (1b) and change in fluorescence was monitored. Data are fit to equation (1) with a K_d of 0.4 nM and an n of 3.6 protein molecules/oligonucleotide. (d) RNA-stimulated ATP hydrolysis in the presence of 5 mM MgCl₂. Steady-state rates of ATP hydrolysis with initial ATP concentrations of 0.1 mM (squares), 0.2 mM (triangles), 0.4 mM (diamonds), 0.8 mM (circles), 1.6 mM (X), and 2.0 mM ATP (+) at various poly(U) RNA concentrations. Data are fit to equation (3) with the constants listed in Scheme 1, and K_{ATP} of 2 mM and K_{RNA} of 3 nM. (e) Initial rates of ATP hydrolysis at various ATP concentrations in the absence of metal without GTP (squares) and with 0.5 mM GTP (triangles). Data are fit to an equation for competitive inhibition with a K_i of GTP of (0.42 mM). A Lineweaver–Burke plot is shown in the inset. (f) Steady-state rates of GTP hydrolysis at 5 (squares), 15 (triangles), 50 (diamonds), 200 (circles) 1000 (x) μ M MgCl₂. Data are fit to equation (4) with constants in Scheme 1 and a K_i (GTP) of 0.42 mM.

the same for MgATP and MgGTP. Once K_1 , K_2 , K_{13} were known, K_5 and K_7 could be calculated from the relationships, $K_{13}K_{15}/K_1 = K_5$ and $K_{13}K_{15}/K_2 = K_7$.

After the dissociation constants were uncovered for three sides of the cube, the constants on the right side could be calculated using the following relationships. K_{11} was calculated from the relationship $K_5K_{12}/K_6 = K_{11}$. K_{14} was calculated from the relationship $K_{13}K_{12}/K_3 = K_{14}$. K_{10} was calculated

from the relationship $K_7K_{12}/K_9 = K_{10}$. Finally, K_8 was calculated from the relationship $K_2K_9/K_3 = K_8$.

Additional titrations were done to check whether several constants were reasonable. For example, K_4 was approximated by analyzing initial rate of ATP hydrolysis at saturating levels of RNA (1 mM). Analysis of three ATP titrations using the Michaelis–Menten equation yielded a K_m of 3.4(\pm 1) mM, which is in accord with the K_4 value of 4.6 mM (Figure 4(a)). Similarly, titrations with ATP in the absence of

RNA but in the presence of optimal metal concentrations (~ 5 mM), yielded K_m values ranging from $1 \mu\text{M}$ – $5 \mu\text{M}$,^{13,34} which are similar to the values of K_7 and K_{13} determined in the global fits (Figure 4(a)).

More titrations with RNA were performed to check K_6 and K_{12} in Scheme 1. With 5 mM MgCl_2 present, three independent titrations revealed that $131(\pm 43)$ nM of RNA was needed to stimulate half maximal rates of ATP hydrolysis, a figure near that determined for K_{12} (218 nM) in the global fits. In the absence of metal, however, repeated RNA titrations showed that $13(\pm 2)$ nM of RNA was needed to stimulate ATPase to half maximum rates (at 2 mM ATP). This value is significantly lower than K_{12} but only begins to approach the K_6 in Scheme 1 (0.37 nM) possibly because 2 mM ATP is not sufficient to saturate the enzyme under the experimental conditions.

Additional titrations with Mg^{2+} were performed to check K_5 and K_{11} . The amount of metal needed to stimulate half-maximal rates of ATP hydrolysis without RNA was normally between $1 \mu\text{M}$ and $20 \mu\text{M}$, which is somewhat higher than K_5 (0.75 μM). The discrepancy can be accounted for by assuming that since enzyme binds ATP weakly without metal, it was not completely saturated during the course of the experiment. Analysis of the amount of metal needed to stimulate half-maximal rates of ATP hydrolysis (at 2 mM ATP) in the presence of 1 mM RNA, where ATP binds more weakly, gave a value of $130(\pm 40) \mu\text{M}$, which is in more reasonable agreement with the K_{11} in Scheme 1 (266 μM).

Binding of free ATP and free Mg^{2+} inhibits DNA unwinding

There has been some debate in the HCV literature as to whether or not ATP hydrolysis is needed to fuel strand separation. Several authors have suggested that ATP hydrolysis is not necessary based on the fact that some mutants defective in ATPase retain some unwinding activity,⁴⁰ some ATPase inhibitors do not abolish unwinding,⁴² and because in some assays HCV helicase appears to separate DNA without ATP.²⁶ Directly testing such a proposal is difficult because most helicase assays are performed under conditions where enzyme far exceeds DNA, and ATPase assays are normally performed under steady-state conditions where enzyme is limiting. Scheme 1 predicts that free metal and free ATP would compete with MgATP when the enzyme is unwinding RNA or DNA. Since metal is absolutely required for unwinding to occur, it is conceivable that both free metal and free ATP inhibit unwinding when they bind blocking the binding of MgATP . Thus, if MgATP were the true substrate needed to fuel unwinding, steady-state unwinding rates should increase with ATP concentration until ATP concentrations exceed total metal concentration, when unwinding rates should decrease.

To test this hypothesis, we used a helicase assay that was recently described by Boguszevska-Chachulska *et al.*³³ to measure unwinding rates under steady-state conditions at numerous ATP and MgCl_2 concentrations. This assay employs a fluorescently labeled DNA substrate composed of a shorter strand labeled on its 3' end with Cy3 dye annealed to a longer strand with Black Hole Quencher 2 (Integrated DNA technologies) attached to its 5' end (Figure 6(a)). Unwinding of this substrate leads to an increase in Cy3 fluorescence (Figure 6(b)). In order for this assay to be used with a limiting concentration of enzyme a third DNA strand must be added along with the ATP to initiate the reaction and also to prevent the Cy3-labeled strand from annealing to the strand with the quencher. In the presence of this "substrate trap" the reaction rates are linear with enzyme concentration and excess trap does not inhibit the reaction. Under such conditions, reactions can be performed where DNA substrate concentrations exceed helicase concentrations.³³

Using this continuous helicase assay, we have measured the relative rates of unwinding at different concentrations of ATP and MgCl_2 . This fluorescence resonance energy transfer (FRET)-based assay is quite robust and allows the measurements of rates that differ by several orders of magnitude (Figure 6(b)). To simulate inhibition of free metal and free ATP, while treating MgATP as the substrate fueling the unwinding reaction, the rates were fit to equation (5). Equation (5) is related to equation (4) except that it uses a new constant to describe the binding of MgATP to the enzyme. This is necessary because it is not clear whether MgATP binds to free enzyme (K_{13}) or an enzyme–DNA complex (analogous to K_{14}) while it unwinds DNA. Reasonable fits were obtained to equation (4) using the K_1 , K_2 and K_{15} described in Scheme 1, and a value for K_{MgATP} of 350 μM (Figure 6), which falls almost equally between the tight binding of MgATP to free enzyme (K_{13} , 2 μM) and the weak binding of MgATP to an enzyme–RNA complex (K_{14} , 20 mM).

The main deviation between our model and the actual data occurs at high metal concentrations where rates are slower than expected when ATP concentrations approach metal concentrations (Figure 6(g) and (h)). Lower than expected unwinding at high metal concentrations may be due to non-specific effects (such as solution ionic strength) unrelated to Mg^{2+} or ATP binding to the Walker NTP-binding site on the helicase. Also, the model predicts somewhat lower rates at some Mg^{2+} concentrations (e.g. Figure 6(e)). These individual fits can be improved simply by changing the equilibrium constants from the ones in Scheme 1 or by using a more robust model that takes into account more steps in unwinding, each of which could be influenced by metal ions. Such a detailed scheme is a future goal, but it will require many more experiments not germane to our present goal of how metal ions interact at the ATP-binding site. Nevertheless, it is interesting to note how unwinding rates follow roughly the same pattern predicted

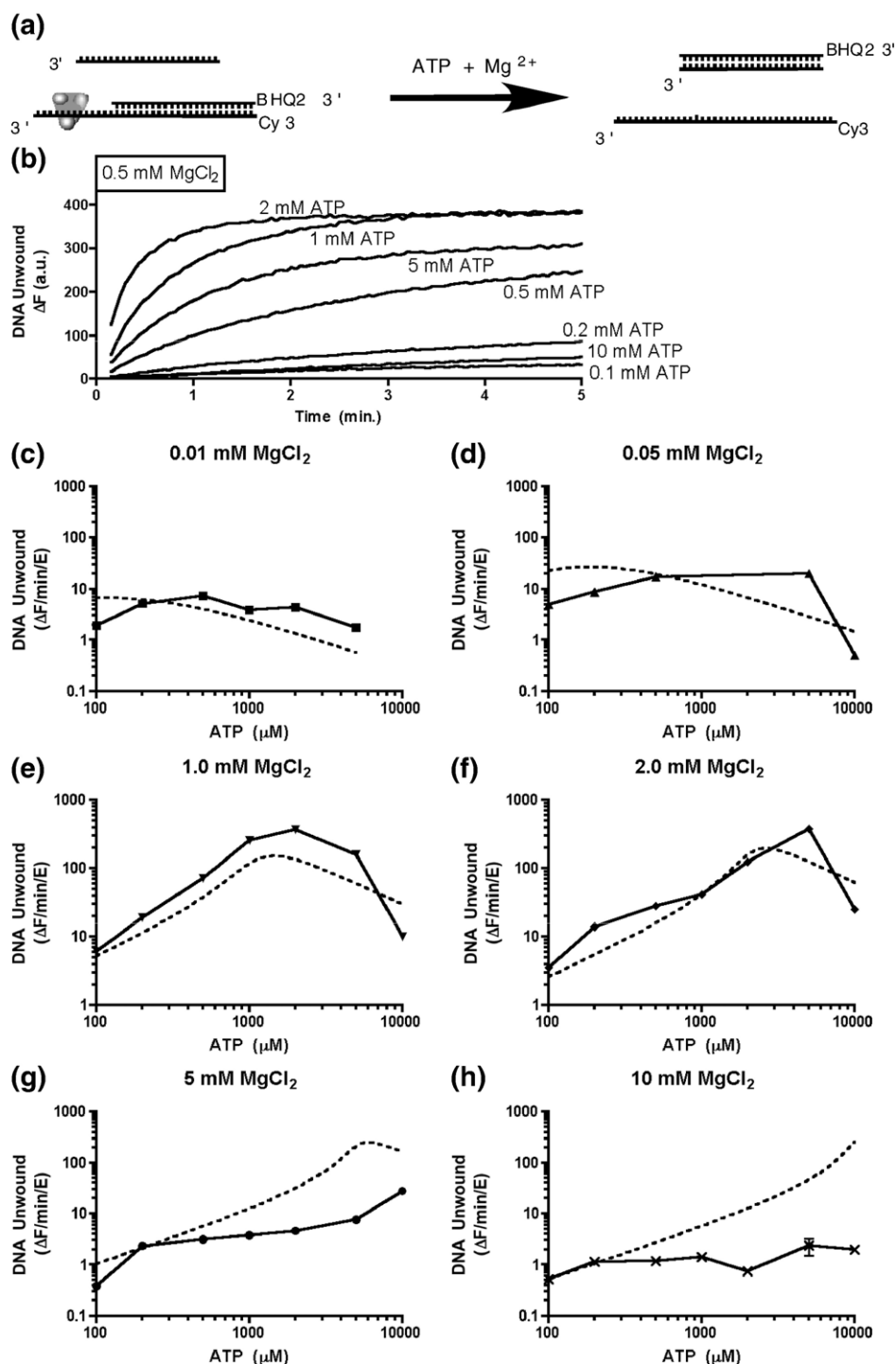


Figure 6. Free ATP and Mg²⁺ inhibit DNA unwinding catalyzed by HCV helicase. (a) Assay used to measure steady-state rates of unwinding at various ATP and Mg²⁺ concentrations. (b) DNA unwinding with 20 nM substrate, 10 nM helicase (Hel-1b), 0.5 mM MgCl₂, and various concentrations of ATP. Initial rates of DNA unwinding in 0.01 mM (c), 0.05 mM (d), 0.5 mM (e), 2.0 mM (f), 5 mM (g), and 10 mM (h) MgCl₂. Data in (c) to (h) are globally fit to equation (5) with the K_1 and K_2 in Scheme 1, a K_{MgATP} of 350 μM and a V_{max} of 450 arbitrary units/min.

by a model based only on MgATP binding and ATP hydrolysis.

Discussion

All motor proteins that use ATP to fuel their movements require divalent metal cations, which

coordinate the phosphate groups of ATP in the catalytic site. In Walker-type ATP-binding sites,¹ the Mg²⁺ usually binds ATP to a conserved aspartate that is near another acidic residue that serves as a catalytic base to activate the water molecule that participates in the hydrolysis. The results described above confirm that such a relationship exists in the helicase encoded by

HCV and also point out some finer details as to how ATP fuels unwinding in this class of enzymes. First, our results show that HCV helicase binds NTPs both in the presence and absence of divalent metal cations. Second, unlike other helicases that have been examined in this detail, the HCV protein will hydrolyze ATP in the absence of metal. Binding and hydrolysis occur at the same site both in the presence and absence of metal, with E291 serving as a putative catalytic base. The NTP binds in a different conformation in the presence and absence of metal. In the presence of metal, NTPs bind tighter and metal ions bind weaker to a D290N mutant, implying that Mg^{2+} binds to D290 forming a bridge to the ATP and reorients the base of the NTP. The 15 dissociation constants and four rate constants in Scheme 1 represent a self-consistent set of parameters that account for all available data. The parameters can be used to predict effects of Mg^{2+} and RNA on helicase catalyzed ATP hydrolysis and steady-state rates of DNA unwinding, demonstrating that the true fuel for the motor function of the enzyme is MgATP.

The interaction of metal ions with helicases has not been widely examined despite the fact that members of this class of ATPases play critical roles in most nucleic acid transactions. Genetically, helicases are classified into families and superfamilies. Helicases in superfamilies 1 and 2 bind and hydrolyze ATP between two RecA-like domains linked in tandem on the same polypeptide. Superfamily 3 and a few other helicase families often function as rings of subunits, each of which contains one RecA-like domain. HCV helicase is a member of superfamily 2. Studies with the ring helicase from bacteriophage T7 have shown that the T7 protein binds NTPs in the absence of metals, and NTP binding facilitates ring formation. In the absence of metal, NTPs are not hydrolyzed, however.³⁵ Soultanas *et al.* have studied the role of metal in ATP hydrolysis catalyzed by a helicase more closely related to HCV Helicase, the PcrA helicase from *Bacillus stearothermophilus*.⁴³ By examining crystal structures of PcrA in the presence and absence of Mg^{2+} and a non-hydrolyzable analog, Soultanas *et al.* proposed that DNA binding to PcrA leads to movement of the conserved lysine in the Walker A motif, so that metal can bind to activate hydrolysis. Our data are not in accord with such a model because we find that the affinity of HCV helicase for metal decreases upon RNA binding. The difference may be due to the fact that PcrA is a member of superfamily 1 and HCV helicase, as a member of superfamily 2, functions somewhat differently.

Our data support a model in which the helicase binds ATP weakly in the absence of metal, and metal binding reorients and stabilizes ATP binding in the absence of RNA ($K_7, K_{13} \ll K_1$). RNA binding in turn destabilizes the enzyme-ATP (or enzyme- Mg^{2+} -ATP) complex by decreasing the affinity of the protein for the metal ion ($K_{10}, K_{14} \gg K_{13}, K_7$). The

acceleration of k_{cat} upon metal binding is likely due to the stabilization of the enzyme-NTP complex, whereas the acceleration of k_{cat} due to RNA binding instead is more likely due to something else, such as stabilization of the transition state or acceleration of product release. Our previous electrostatic analyses of HCV helicase structures provide an explanation for how RNA binding lead to a release of metal.⁴⁴ In the absence of nucleic acid D290 is negatively charged as would be expected. However, in the presence of a bound DNA oligonucleotide D290 has an unusually high pK_a value of 10, meaning that it would be protonated at physiological pH and unable to coordinate a cation.

The metal-independent NTPase activity of HCV helicase reported here needs to be interpreted cautiously because such activity is not normally seen with enzymes possessing Walker NTP binding sites. The D290N and E291Q mutants were originally constructed because we thought that either the wild-type enzyme was contaminated or there was a second ATP-binding site on HCV helicase. The fact that the mutant enzymes are ~1000 times less active than the wild-type (without metal) when all three enzymes were expressed and purified with identical procedures and free of any other visible bands on SDS-containing gels argues strongly against either notion (Figure 3). Furthermore, if the wild-type were contaminated or had a second active site, it is highly unlikely RNA/DNA would stimulate a second active site (Figure 5(b)). There is still the possibility that the wild-type enzyme co-purifies with some tightly bound metal and that a second metal ion binds with ATP, but nevertheless, our data show that in the absence of such added metal, NTPs bind weaker leading to slower hydrolysis of some NTPs.

Our conclusion that the divalent metal cation forms a bridge between D290 and the phosphates of ATP is based on the facts that (1) the D290N mutant does not unwind DNA and requires dramatically more Mg^{2+} to activate its ATP hydrolysis, and (2) the wild-type protein binds ATP more tightly when Mg^{2+} is bound ($K_7 < K_1, K_{10} < K_4$). Coordination of metal to an Asp in the Walker B site (analogous to D290) has been observed in structures of related helicases.^{27,29,30} Although high-resolution structures of HCV helicase bound to MgATP are not yet available it appears that, in this case, HCV helicase fits the current paradigm with regard to metal ion coordination. The fact that D290N loses ATPase activity even in the absence of metal suggests the residue has a second role in addition to binding metal. For example, the charged state of D290 undoubtedly influences the electrostatics of its neighboring residue E291.

The adjacent residue E291 is homologous to residues in other ATPases that serve as catalytic bases.^{39,45,46} The data obtained with the E291Q mutant explain why such a mutant cannot unwind RNA and are in accord with a role as a catalytic base. The fact that this mutation affects ATP hydrolysis both in the presence and absence of

metal demonstrates that NTP binds the same site both in the presence and absence of metal. Thus, this study does not support the notion that there is more than one ATPase site on HCV helicase. Others have suggested that HCV helicase might contain two distinct ATP binding sites based on inhibitor studies²⁴ and an apparent cooperativity in ATP binding.²⁵

Scheme 1 also provides a simple explanation for the seemingly unusual regulation of the HCV helicase by ATP, which could be mistakenly interpreted as cooperative ATP binding if one does not take metal ions into account. Our data show that lower than expected unwinding at low and high ATP concentrations need not be due to anything besides the unproductive binding of free ATP or Mg^{2+} to the enzyme. Although our data do not support models involving the helicase acting as a dimer or higher order oligomer, which would imply cooperation or coordination of ATP binding sites on adjacent subunits, they do not directly rule out such possibilities. Nevertheless, our results are more in accord with models that contend that the helicase stretches and contracts to move like an inchworm as a monomer with only one non-cooperative ATP-binding site. Thus, our model contends that each helicase hydrolyzes ATP as a monomer with Mg^{2+} and RNA activating hydrolysis by binding a single site on the enzyme. This 1:1:1 stoichiometry is supported by structural data for HCV helicase, which reveal a single ssDNA binding site^{15,19} and structures of related helicases, which show a single metal ion coordinating ATP.^{27,29} In contrast with some previous studies,^{24,25} this analysis of the NS3 helicase fragment (Hel-1b) does not reveal any evidence for more than one ATP binding site. The difference may be due to the fact that we utilized a truncated NS3 protein, which might behave somewhat differently from the full-length NS3 protein. Likewise, we have yet to find any evidence that more than one Mg^{2+} is needed to coordinate ATP hydrolysis. All plots of rates *versus* metal ion concentration fit one site binding models better than two site models or those using Hill equations, and plots of rates *versus* MgATP reveal simple Michaelis–Menten kinetics, with a V_{max} not stimulated by additional Mg^{2+} . Nevertheless, it will be important in the future to verify this stoichiometry by directly examining metal binding to HCV helicase using NMR or another biophysical technique.

Although Scheme 1 provides a thermodynamically sound basis to now study the mechanism of action of HCV helicase catalyzed ATP hydrolysis, it does have some limitations that need to be noted. First, only half of the equilibrium constants were determined from fits to experimental data and the rest were calculated assuming thermodynamic reciprocity. Five of the calculated constants (K_4 , K_5 , K_6 , K_{11} , K_{16}) were checked by performing addition titrations and measuring ATP hydrolysis. All were in reasonable agreement with the calcu-

lated values except K_5 and K_6 , each of which represented about a tenfold difference from the calculated values. While it is possible that the individual titrations were not performed under appropriate conditions, it is also possible that additional states exist limiting reciprocity. For example, the E^{A^*} complex might not be able to directly convert to an E^{MA} complex. On a similar note, only K_9 was determined here by direct binding assays (Figure 5(c)). Several others constants are, nevertheless, in reasonable agreement with binding assays. For example if K_2 is estimated from direct binding (Figure 5(a)), the result is ~ 0.025 nM, which is near the value determined with kinetics (0.014 nM). Likewise, several groups have estimated K_{12} previously using a non-hydrolyzable ATP analog.^{47–49} The resulting values range from 10 μ M–580 μ M and cover the range of the kinetically determined K_{12} in Scheme 1 (218 μ M). Last, it should be noted that the Scheme implies only a 24-fold weakening of RNA binding in the presence of Mg^{2+} (K_3 *versus* K_9) and a 589-fold weakening by Mg^{2+} when ATP is present (K_6 *versus* K_{12}), even though it is well established that increasing Mg^{2+} continuously decreases the affinity of enzymes for nucleic acids. Our interpretation of metal ion effects on enzyme–RNA binding does not explain the full effect because Scheme 1 only relates Mg^{2+} binding to one site. Scheme 1 does not take into account binding of additional metal ions to other sites (or non-specific sites) on either the enzyme or RNA. If it did, then it would better explain this effect and, as mentioned in Results, the resulting lower than expected unwinding activity at high metal concentrations.

Finally, the fact that HCV helicase binds free ATP in a conformation somewhat different from that of MgATP binding is of practical importance because it suggests the possibility that nucleotide-based inhibitors could be synthesized that trap the enzyme in a non-productive enzyme–NTP or enzyme–RNA–NTP complex. Likewise, it appears that some metals might be found that bind near D290 to prevent the binding of the MgATP complex. Such inhibitors could form the basis for novel and much needed treatments for the hepatitis C epidemic.

Materials and Methods

Materials

DNA oligonucleotides were purchased from Integrated DNA Technologies (Coralville, IA), and their concentrations were determined from provided extinction coefficients. The NS3–NS4A complex, and the truncated NS3 proteins called Hel-1a, Hel-1b, and Hel-2a have been described.^{13,34} The Hel-1b and its mutants (D290N and E291Q) contained NS3 amino acid residues 166–631 from genotype 1b followed by a C-terminal His-tag with the sequence PNS SSV DKL AAA LEH HHH HH. NS3 proteins were purified as described^{13,34} and protein

concentrations were determined by using A_{280} with the extinction coefficients calculated from the Trp, Tyr, and Phe content of each protein. It should be noted that after purification on a Ni-NTA column, the truncated proteins were purified using two additional columns (gel filtration and ion exchange) both performed in the in buffers containing EDTA.

Site-directed mutagenesis

The Quik Change site-directed mutagenesis kit (Stratagene, La Jolla, CA) was used to construct each mutant from the plasmid p24Hel-1b, which contains the helicase region of NS3. The following oligonucleotides were utilized in this PCR-based mutagenesis: D290N(+)
cc tat gac atc ata ata tgt aat gag tgc cac tca act gac, D290N(-)
gtc agt tga gtg gca ctc att aca tat tat gat gtc ata g, E291Q(+)
gac atc ata ata tgt gat cag tgc cac tca act gac tgc, E291Q(-)
cga gtc agt tga gtg gca ctg atc aca tat tat gat gtc. Mutations were confirmed by sequencing the plasmid DNA.

$$\Delta F = \Delta F_{\text{MAX}} \frac{(K_D + [E]_T/n + [\text{DNA}]_T) - \sqrt{(K_D + [E]_T/n + [\text{DNA}]_T)^2 - 4[E]_T[\text{DNA}]_T/n}}{2[\text{DNA}]_T} \quad (1)$$

ATPase assay

A modified “malachite green” assay was performed at 37 °C in presence of 25 mM Mops (pH 6.5), 0.1% (v/v) Tween 20, MgCl_2 , ATP at indicated concentrations and catalytic amount of helicase (1 nM–50 nM). Reactions (100 μl) were terminated with the addition of 0.2 ml of freshly prepared 3:1 mixture of 0.045% (w/v) malachite green and 0.42% (w/v) ammonium molybdate in 1 M H_2SO_4 . Within seconds, 25 μl of sodium citrate was added to the solution to increase the pH of the reaction so that the ATP was not subject to acidic environment. After incubation for 20 min at room temperature, the absorbance was measured at 630 nm.

DNA binding assay

The binding of a fluorescein-labeled DNA oligonucleotide F18 to HCV helicase was monitored as described.¹³ Solutions (2 ml) containing 1 nM or 2 nM oligonucleotide in 25 mM Mops (pH 6.5), 5 mM MgCl_2 , and 0.1% Tween 20 were titrated with recombinant helicase (Hel-1b, D290N, or E291Q). Fluorescence was measured at an excitation wavelength of 492 nm and an emission of 518 nm with a Varian Carey Eclipse fluorescence spectrophotometer.

FRET-based helicase assay

Fluorescent helicase substrates were used to measure unwinding rates as described³³ using an assay based on well-established fluorescence-based helicase assays.^{50–52} Reactions were performed in 25 mM Mops (pH 6.5), 25% (v/v) glycerol, 0.1% Tween 20, 1 mM DTT, 20 nM DNA substrate, 200 nM “trap” DNA oligonucleotide, 10 nM helicase, and ATP and MgCl_2 at indicated concentrations. All reactions were conducted at 37 °C in a reaction volume of 100 μl with a substrate composed of a Cy3-labeled long strand (Cy3-TAG TAC CGC CAC CCT CAG AAC CTT TTT TTT TTT TTT-3') annealed to a short strand tagged

with black hole quencher 2 (5'-GGT TCT GCG GGT GGC GGT ACT A-BHQ2). The trap strand was the complement to the short strand (5'-TAG TAC CGC CAC CCT CAG AAC C-3'). Fluorescence was measured using a Varian Cary Eclipse fluorescence spectrophotometer with excitation and emission wavelengths set for 550 nm and 570 nm, respectively, and slit widths set to 10 nm for both the excitation and emission. Initial velocities were calculated using linear regression with datasets pruned of values outside the linear range.

Data analysis

The constants in Scheme 1 were determined as follows. First, direct binding assays were used to determine K_D and estimate K_3 . Binding isotherms were obtained with two different concentrations of oligonucleotide and fit to equation as described above and the data fit to equation (1) using global non-linear regression (Graphpad Prism, San Diego, CA):

where ΔF_{MAX} is the maximum fluorescence change of each titration. The factor n represents the number of protein monomers bound to a single oligonucleotide, and K_D represents K_D when Mg^{2+} is present at saturating levels (Figure 5(c)), and K_3 when Mg^{2+} is absent (Figure 5(a)). Each set of two titrations was repeated three times and errors in scheme 1 represent the standard deviations of K_D values determined from three separate global fits.

Steady-state ATPase assays were then conducted at various ATP concentrations in the absence of Mg^{2+} and RNA and fit to the Michaelis–Menten equation with the K_m defined as K_1 . The ATP titration was repeated five times and the average K_1 and k_{cat} are listed in Scheme 1 with a standard deviation defined by five independent experiments. Next, ATPase assays were performed at various ATP and RNA concentrations (in the absence of Mg^{2+}) and the amount of ATP cleaved after 15 and 30 min was measured. Average rates were fit to equation (2) (Figure 5(b)):

$$\frac{v}{E_T} = \frac{k_{\text{cat}} \frac{[\text{ATP}]}{K_1} + \beta k_{\text{cat}} \frac{[\text{RNA}][\text{ATP}]}{K_6 K_1}}{1 + \frac{[\text{ATP}]}{K_1} + \frac{[\text{RNA}]}{K_3} + \frac{[\text{RNA}][\text{ATP}]}{K_6 K_1}} \quad (2)$$

where all constants are defined in scheme 1 (Figure 4(a)). In the fit, limits were placed on K_3 based on the results of the above binding experiments (K_3 was only allowed to vary between 0 and 1 nM). K_1 was set to a constant. Each set of six titrations was repeated three times and the errors represent the standard deviations of K_3 and K_6 determined from three separate global fits.

To determine the affinity of the protein for RNA in the presence of saturating Mg^{2+} , the above titrations (three sets) were repeated in the presence of 5 mM MgCl_2 , and fit to equation (3) (Figure 5(d)):

$$\frac{v}{E_T} = \frac{\alpha k_{\text{cat}} \frac{[\text{ATP}]}{K_{\text{ATP}}} + \gamma k_{\text{cat}} \frac{[\text{RNA}][\text{ATP}]}{K_{12} K_{\text{ATP}}}}{1 + \frac{[\text{ATP}]}{K_{\text{ATP}}} + \frac{[\text{RNA}]}{K_{\text{RNA}}} + \frac{[\text{RNA}][\text{ATP}]}{K_{12} K_{\text{ATP}}}} \quad (3)$$

Each set of six titrations was repeated twice and the errors represent the standard deviations of K_{12} determined from two separate global fits.

Next, solutions with various Mg^{2+} concentrations were titrated with GTP, and its rate of hydrolysis was measured at two different time points. The average velocity under each condition was plotted and fit to equation (4) (Figure 5(f)):

$$\frac{v}{E_T} = \frac{\alpha k_{cat}}{\left(1 - \frac{K_{13}}{K_1} - \frac{K_{13}}{K_2}\right) + \left(1 + \frac{[GTP]_T}{K_1} + \frac{[Mg^{2+}]_T}{K_2}\right) \frac{2K_{13}}{([Mg^{2+}]_T + [GTP]_T + K_{15}) - \sqrt{([Mg^{2+}]_T + [GTP]_T + K_{15})^2 - 4[Mg^{2+}][GTP]_T}}}$$
(4)

In the global fit, only K_2 and K_{13} were allowed to vary. K_1 was the K_i determined for GTP in competition experiments done *versus* ATP in the absence of metal (Figure 5(e)). The titration sets were repeated three times and the errors represent the standard deviations of K_2 and K_{13} determined from three separate global fits. For this analysis, K_{15} was set at 83 μ M.⁵³

The other constants in Scheme 1 were calculated using the following relationships: $K_4 = K_1 K_6 / K_3$, $K_5 = K_{13} K_{15} / K_1$, $K_7 = K_{13} K_{15} / K_2$, $K_8 = K_2 K_9 / K_3$, $K_{10} = K_7 K_{12} / K_9$, $K_{11} = K_5 K_{12} / K_6$, and $K_{14} = K_{13} K_{12} / K_3$. Note that K_4 , K_5 , K_7 , K_8 , and K_{14} are all calculated from three experimentally determined parameters, whereas K_{10} and K_{11} are calculated from two experimentally determined parameters and one calculated parameter, which was in turn determined from three experimentally determined parameters. For the calculated parameters, the errors are based upon the largest error of the three known parameters. For example, in calculating K_4 , K_6 had a 48% uncertainty, which was larger than the uncertainty for either K_1 (18%) or K_3 (34%). Thus, K_4 was given a 48% uncertainty.

Unwinding data were fit to the following equation using non-linear least-squares analysis using Graphpad Prism software (San Diego, CA):

$$v = \frac{V_{max}}{\left(1 - \frac{K_{MgATP}}{K_1} - \frac{K_{MgATP}}{K_2}\right) + \left(1 + \frac{[ATP]_T}{K_1} + \frac{[Mg^{2+}]_T}{K_2}\right) \frac{2K_{MgATP}}{([Mg^{2+}]_T + [ATP]_T + K_{15}) - \sqrt{([Mg^{2+}]_T + [ATP]_T + K_{15})^2 - 4[Mg^{2+}][ATP]_T}}}$$
(5)

In this fit, K_1 and K_2 were set to the values in Scheme 1 and only V_{max} and K_{MgATP} were allowed to vary.

Acknowledgements

We thank Fred Jaffe, Christopher M. Frenz, and Angela M.I. Lam for valuable technical assistance. National Institutes of Health grant AI052395 supported this work.

References

1. Walker, J. E., Saraste, M., Runswick, M. J. & Gay, N. J. (1982). Distantly related sequences in the alpha- and

beta-subunits of ATP synthase, myosin, kinases and other ATP-requiring enzymes and a common nucleotide binding fold. *EMBO J.* **1**, 945–951.

2. Dumont, S., Cheng, W., Serebrov, V., Beran, R. K., Tinoco, I. J., Pyle, A. M. & Bustamante, C. (2006). RNA translocation and unwinding mechanism of HCV NS3 helicase and its coordination by ATP. *Nature*, **439**, 105–108.
3. Piccininni, S., Varaklioti, A., Nardelli, M., Dave, B., Raney, K. D. & McCarthy, J. E. (2002). Modulation of the hepatitis C virus RNA-dependent RNA polymerase activity by the non-structural (NS) 3 helicase and the NS4B membrane protein. *J. Biol. Chem.* **277**, 45670–45679.
4. Lam, A. M. & Frick, D. N. (2006). Hepatitis C virus subgenomic replicon requires an active NS3 RNA helicase. *J. Virol.* **80**, 404–411.
5. Frick, D. N. (2003). Helicases as antiviral drug targets. *Drug News Perspect.* **16**, 355–362.
6. Kwong, A. D., Rao, B. G. & Jeang, K. T. (2005). Viral and cellular RNA helicases as antiviral targets. *Nature Rev. Drug Discov.* **4**, 845–853.
7. Frick, D. N. & Lam, A. M. (2006). Understanding helicases as a means of virus control. *Curr. Pharm. Des.* **12**, 1315–1338.
8. Tomei, L., Failla, C., Santolini, E., De Francesco, R. & La Monica, N. (1993). NS3 is a serine protease required for processing of hepatitis C virus polyprotein. *J. Virol.* **67**, 4017–4026.
9. Suzich, J. A., Tamura, J. K., Palmer-Hill, F., Warren, P., Grakoui, A., Rice, C. M. *et al.* (1993). Hepatitis C virus NS3 protein polynucleotide-stimulated nucleoside triphosphatase and comparison with the related pestivirus and flavivirus enzymes. *J. Virol.* **67**, 6152–6158.
10. Grakoui, A., McCourt, D. W., Wychowski, C., Feinstone, S. M. & Rice, C. M. (1993). Characterization of the hepatitis C virus-encoded serine proteinase: determination of proteinase-dependent polyprotein cleavage sites. *J. Virol.* **67**, 2832–2843.
11. Tai, C. L., Chi, W. K., Chen, D. S. & Hwang, L. H. (1996). The helicase activity associated with hepatitis C virus non-structural protein 3 (NS3). *J. Virol.* **70**, 8477–8484.
12. Gwack, Y., Kim, D. W., Han, J. H. & Choe, J. (1997). DNA helicase activity of the hepatitis C virus non-structural protein 3. *Eur. J. Biochem.* **250**, 47–54.
13. Frick, D. N., Rypma, R. S., Lam, A. M. & Gu, B. (2004). The non-structural protein 3 protease/helicase

- requires an intact protease domain to unwind duplex RNA efficiently. *J. Biol. Chem.* **279**, 1269–1280.
14. Cho, H. S., Ha, N. C., Kang, L. W., Chung, K. M., Back, S. H., Jang, S. K. & Oh, B. H. (1998). Crystal structure of RNA helicase from genotype 1b hepatitis C virus. A feasible mechanism of unwinding duplex RNA. *J. Biol. Chem.* **273**, 15045–15052.
 15. Kim, J. L., Morgenstern, K. A., Griffith, J. P., Dwyer, M. D., Thomson, J. A., Murcko, M. A. *et al.* (1998). Hepatitis C virus NS3 RNA helicase domain with a bound oligonucleotide: the crystal structure provides insights into the mode of unwinding. *Structure*, **6**, 89–100.
 16. Yao, N., Reichert, P., Taremi, S. S., Prosser, W. W. & Weber, P. C. (1999). Molecular views of viral poly-protein processing revealed by the crystal structure of the hepatitis C virus bifunctional protease-helicase. *Struct. Fold. Des.* **7**, 1353–1363.
 17. Yao, N., Hesson, T., Cable, M., Hong, Z., Kwong, A. D., Le, H. V. & Weber, P. C. (1997). Structure of the hepatitis C virus RNA helicase domain. *Nature Struct. Biol.* **4**, 463–467.
 18. Story, R. M. & Steitz, T. A. (1992). Structure of the recA protein-ADP complex. *Nature*, **355**, 374–376.
 19. Mackintosh, S. G., Lu, J. Z., Jordan, J. B., Harrison, M. K., Sikora, B., Sharma, S. D. *et al.* (2006). Structural and biological identification of residues on the surface of NS3 helicase required for optimal replication of the hepatitis C virus. *J. Biol. Chem.* **281**, 3528–3535.
 20. Porter, D. J., Short, S. A., Hanlon, M. H., Preugschat, F., Wilson, J. E., Willard, D. H. J. & Consler, T. G. (1998). Product release is the major contributor to k_{cat} for the hepatitis C virus helicase-catalyzed strand separation of short duplex DNA. *J. Biol. Chem.* **273**, 18906–18914.
 21. Levin, M. K., Wang, Y. H. & Patel, S. S. (2004). The functional interaction of the hepatitis C virus helicase molecules is responsible for unwinding processivity. *J. Biol. Chem.* **279**, 26005–26012.
 22. Tackett, A. J., Chen, Y., Cameron, C. E. & Raney, K. D. (2005). Multiple full-length NS3 molecules are required for optimal unwinding of oligonucleotide DNA in vitro. *J. Biol. Chem.* **280**, 10797–10806.
 23. Serebrov, V. & Pyle, A. M. (2004). Periodic cycles of RNA unwinding and pausing by hepatitis C virus NS3 helicase. *Nature*, **430**, 476–480.
 24. Porter, D. J. (1998). Inhibition of the hepatitis C virus helicase-associated ATPase activity by the combination of ADP, NaF, MgCl₂, and poly(rU). Two ADP binding sites on the enzyme-nucleic acid complex. *J. Biol. Chem.* **273**, 7390–7396.
 25. Locatelli, G. A., Spadari, S. & Maga, G. (2002). Hepatitis C virus NS3 ATPase/helicase: an ATP switch regulates the cooperativity among the different substrate binding sites. *Biochemistry*, **41**, 10332–10342.
 26. Porter, D. J. & Preugschat, F. (2000). Strand-separating activity of hepatitis C virus helicase in the absence of ATP. *Biochemistry*, **39**, 5166–5173.
 27. Velankar, S. S., Soutanas, P., Dillingham, M. S., Subramanya, H. S. & Wigley, D. B. (1999). Crystal structures of complexes of PcrA DNA helicase with a DNA substrate indicate an inchworm mechanism. *Cell*, **97**, 75–84.
 28. Singleton, M. R., Sawaya, M. R., Ellenberger, T. & Wigley, D. B. (2000). Crystal structure of T7 gene 4 ring helicase indicates a mechanism for sequential hydrolysis of nucleotides. *Cell*, **101**, 589–600.
 29. Bernstein, D. A., Zittel, M. C. & Keck, J. L. (2003). High-resolution structure of the *E. coli* RecQ helicase catalytic core. *EMBO J.* **22**, 4910–4921.
 30. Sengoku, T., Nureki, O., Nakamura, A., Kobayashi, S. & Yokoyama, S. (2006). Structural basis for RNA unwinding by the DEAD-box protein *Drosophila vasa*. *Cell*, **125**, 287–300.
 31. Kim, D. W., Gwack, Y., Han, J. H. & Choe, J. (1995). C-terminal domain of the hepatitis C virus NS3 protein contains an RNA helicase activity. *Biochem. Biophys. Res. Commun.* **215**, 160–166.
 32. Wardell, A. D., Errington, W., Ciaramella, G., Merson, J. & McGarvey, M. J. (1999). Characterization and mutational analysis of the helicase and NTPase activities of hepatitis C virus full-length NS3 protein. *J. Gen. Virol.* **80**, 701–709.
 33. Boguszewska-Chachulska, A. M., Krawczyk, M., Stankiewicz, A., Gozdek, A., Haenni, A. L. & Strokovskaya, L. (2004). Direct fluorometric measurement of hepatitis C virus helicase activity. *FEBS Letters*, **567**, 253–258.
 34. Lam, A. M., Keeney, D., Eckert, P. Q. & Frick, D. N. (2003). Hepatitis C virus NS3 ATPases/helicases from different genotypes exhibit variations in enzymatic properties. *J. Virol.* **77**, 3950–3961.
 35. Picha, K. M. & Patel, S. S. (1998). Bacteriophage T7 DNA helicase binds dTTP, forms hexamers, and binds DNA in the absence of Mg²⁺. The presence of dTTP is sufficient for hexamer formation and DNA binding. *J. Biol. Chem.* **273**, 27315–27319.
 36. Wengler, G. & Wengler, G. (1993). The NS 3 non-structural protein of flaviviruses contains an RNA triphosphatase activity. *Virology*, **197**, 265–273.
 37. Bartelma, G. & Padmanabhan, R. (2002). Expression, purification, and characterization of the RNA 5'-triphosphatase activity of dengue virus type 2 non-structural protein 3. *Virology*, **299**, 122–132.
 38. Benarroch, D., Selisko, B., Locatelli, G. A., Maga, G., Romette, J. L. & Canard, B. (2004). The RNA helicase, nucleotide 5'-triphosphatase, and RNA 5'-triphosphatase activities of Dengue virus protein NS3 are Mg²⁺-dependent and require a functional Walker B motif in the helicase catalytic core. *Virology*, **328**, 208–218.
 39. Crampton, D. J., Mukherjee, S. & Richardson, C. C. (2006). DNA-induced switch from independent to sequential dTTP hydrolysis in the bacteriophage T7 DNA helicase. *Mol. Cell*, **21**, 165–174.
 40. Tai, C. L., Pan, W. C., Liaw, S. H., Yang, U. C., Hwang, L. H. & Chen, D. S. (2001). Structure-based mutational analysis of the hepatitis C virus NS3 helicase. *J. Virol.* **75**, 8289–8297.
 41. Segel, I. H. (1975). *Enzyme Kinetics: Behavior and Analysis of Rapid Equilibrium and Steady-State Enzyme Systems*. John Wiley and Sons, Inc., New York.
 42. Zhang, N., Chen, H. M., Koch, V., Schmitz, H., Minczuk, M., Stepien, P. *et al.* (2003). Potent inhibition of NTPase/helicase of the West Nile Virus by ring-expanded ("fat") nucleoside analogues. *J. Med. Chem.* **46**, 4776–4789.
 43. Soutanas, P., Dillingham, M. S., Velankar, S. S. & Wigley, D. B. (1999). DNA binding mediates conformational changes and metal ion coordination in the active site of PcrA helicase. *J. Mol. Biol.* **290**, 137–148.
 44. Frick, D. N., Rypma, R. S., Lam, A. M. & Frenz, C. M. (2004). Electrostatic analysis of the hepatitis C virus NS3 helicase reveals both active and allosteric site locations. *Nucl. Acids Res.* **32**, 5519–5528.

45. Orelle, C., Dalmas, O., Gros, P., Di Pietro, A. & Jault, J. M. (2003). The conserved glutamate residue adjacent to the Walker-B motif is the catalytic base for ATP hydrolysis in the ATP-binding cassette transporter BmrA. *J. Biol. Chem.* **278**, 47002–47008.
46. Zito, C. R., Antony, E., Hunt, J. F., Oliver, D. B. & Hingorani, M. M. (2005). Role of a conserved glutamate residue in the *Escherichia coli* SecA ATPase mechanism. *J. Biol. Chem.* **280**, 14611–14619.
47. Levin, M. K., Gurjar, M. M. & Patel, S. S. (2003). ATP binding modulates the nucleic acid affinity of hepatitis C virus helicase. *J. Biol. Chem.* **278**, 23311–23316.
48. Lam, A. M., Keeney, D. & Frick, D. N. (2003). Two novel conserved motifs in the hepatitis C virus NS3 protein critical for helicase action. *J. Biol. Chem.* **278**, 44514–44524.
49. Lam, A. M., Rypma, R. S. & Frick, D. N. (2004). Enhanced nucleic acid binding to ATP-bound hepatitis C virus NS3 helicase at low pH activates RNA unwinding. *Nucl. Acids Res.* **32**, 4060–4070.
50. Raney, K. D., Sowers, L. C., Millar, D. P. & Benkovic, S. J. (1994). A fluorescence-based assay for monitoring helicase activity. *Proc. Natl Acad. Sci. USA*, **91**, 6644–6648.
51. Houston, P. & Kodadek, T. (1994). Spectrophotometric assay for enzyme-mediated unwinding of double-stranded DNA. *Proc. Natl Acad. Sci. USA*, **91**, 5471–5474.
52. Bjornson, K. P., Amaratunga, M., Moore, K. J. & Lohman, T. M. (1994). Single-turnover kinetics of helicase-catalyzed DNA unwinding monitored continuously by fluorescence energy transfer. *Biochemistry*, **33**, 14306–14316.
53. Williams, G. D., Mosher, T. J. & Smith, M. B. (1993). Simultaneous determination of intracellular magnesium and pH from the three ³¹P NMR chemical shifts of ATP. *Anal. Biochem.* **214**, 458–467.

Edited by D. E. Draper

(Received 31 July 2006; received in revised form 6 October 2006; accepted 8 October 2006)
Available online 13 October 2006